Perceptron learning rule derived from spike-frequency adaptation and spike-time-dependent plasticity

Prashanth D'Souza, Shih-Chii Liu[1], and Richard H. R. Hahnloser

Institute of Neuroinformatics, University of Zurich and ETH Zurich, Winterthurerstrasse 190, Zurich 8057, Switzerland

Edited by Eric I. Knudsen, Stanford University School of Medicine, Stanford, CA, and approved December 14, 2009 (received for review August 19, 2009)

It is widely believed that sensory and motor processing in the brain is based on simple computational primitives rooted in cellular and synaptic physiology. However, many gaps remain in our understanding of the connections between neural computations and biophysical properties of neurons. Here, we show that synaptic spike-time-dependent plasticity (STDP) combined with spike-frequency adaptation (SFA) in a single neuron together approximate the well-known perceptron learning rule. Our calculations and integrate-and-fire simulations reveal that delayed inputs to a neuron endowed with STDP and SFA precisely instruct neural responses to earlier arriving inputs. We demonstrate this mechanism on a developmental example of auditory map formation guided by visual inputs, as observed in the external nucleus of the inferior colliculus (ICX) of barn owls. The interplay of SFA and STDP in model ICX neurons precisely transfers the tuning curve from the visual modality onto the auditory modality, demonstrating a useful computation for multimodal and sensory-guided processing.

delta learning rule | Hebbian learning | sensory fusion | synaptic potentiation | supervised

Many of the sensory and motor tasks solved by the brain can be captured in simple equations or minimization criteria. For example, minimization of errors made during reconstruction of natural images using sparse priors leads to linear filters reminiscent of simple cells (1, 2), minimization of retinal slip or visual error leads to emergence and maintenance of neural integrator networks (3–5), and optimality criteria derived from information theory can model the remapping dynamics of receptive fields in the barn owl midbrain (6).

Despite these advances, little is known about cellular physiological properties that could serve as primitives for solving such computational tasks. Among the known primitives are short-term synaptic depression, which can give rise to multiplicative gain control (7), or spike-frequency adaptation (SFA), which may provide high-pass filtering of sensory inputs (8, 9).

Here, we explore biophysical mechanisms and computational primitives for instructive coding. Instructive coding is a computation that allows the brain to constrain its sensory representations adaptively by exploiting intrinsic properties of the physical world. The example we consider here is that sound sources and salient visual stimuli often co-localize (e.g., when a dried branch cracks under the footstep of an animal). In the barn owl, a highly efficient predator, this auditory–visual co-localization is well reflected by registration of auditory and visual maps in the external nucleus of the inferior colliculus (ICX) and the optic tectum (OT). The instructive aspect of this registration is that it is actively maintained by plasticity mechanisms: When the visual field of owls is chronically shifted by prisms, neurons in ICX and OT develop a shift in their auditory receptive fields that corresponds to the visual field displacement (10, 11). Hence, visual inputs to these areas are able to serve instructive roles for auditory spatial representations.

In the computational literature, instructive coding has been linked to the perceptron rule, a learning rule for one-layer neural network models (12, 13). This rule guarantees that the firing rate approaches the target rate and is one of the simplest expressions of an almost infinite class of learning algorithms that go under the name of gradient descent algorithms. Although the perceptron rule and gradient descent algorithms have been broadly applied to network models of brain function (14–16), to our knowledge, they have not been derived from first principles and abundant experimental evidence for their existence is still lacking. One of the most prominent criticisms is that these algorithms depend on the existence of an explicit error signal, for which convincing evidence is scarce in most neural systems.

A special case of instructive coding, cross-modal spatial transformations, can be formed by spike-time-dependent plasticity (STDP) rules when driven by multimodal inputs (17, 18). Although STDP by itself does not seem to be capable of supporting arbitrary instructive coding (19), we identify a possible scenario for the implementation of the perceptron rule, namely, in cells that display both SFA and STDP. For a large range of parameters, the interaction of these common cellular and synaptic properties gives rise to the perceptron rule and represents a robust mechanism for supervised learning in biological systems. Most importantly, the error signal in our STDP–SFA scenario is implicit rather than explicit, which alleviates the exploratory urge to identify such signals experimentally.

Results

To explore a possible relationship between firing adaptation, STDP, and error signals, we studied a spiking neuron model based on the organization of the owl midbrain and on physiological responses. Our (ICX) model neuron is an adapting conductance-based leaky integrate-and-fire unit in which SFA is modeled by an after-hyperpolarizing potassium conductance (20).

The unit receives excitatory sensory input a from a fast-acting auditory pathway and input v from a slower acting visual pathway (Fig. 1). The auditory-input synapses are subject to STDP, whereas the visual-input synapses are fixed.

Our results are based on numerical simulations, and, to avoid exhaustive parameter testing, we first show analytical results in which we use the method of time averaging to replace spike trains with average firing-rates (see *Analytical Derivation* in *Methods*). This approximation is valid as long as neurons operate over a range of firing rates in which the slopes of their F-I curves do not change much.

SFA Can Encode an Implicit Error Signal. First, we examine the effects of SFA on bimodal neural responses. We stimulate the neuron with auditory and visual stimuli that are step functions of duration T. To model the slower visual pathway, visual inputs (v) have a fixed onset lag of $T_{\mathrm{lat}} = 70$ ms, corresponding to estimates in the barn owl (22). When driven by auditory or visual input in isolation, the neuron

Author contributions: S.-C.L., and R.H.R.H. designed research; P.D. performed research; P.D., S.-C.L., and R.H.R.H. analyzed data; P.D., S.-C.L., and R.H.R.H. wrote the paper.

The authors declare no conflict of interest.

This article is a PNAS Direct Submission.

Freely available online through the PNAS open access option.

[1]To whom correspondence should be addressed at: Institute of Neuroinformatics, University of Zurich, Winterthurerstrasse 190, Zurich 8057, Switzerland. E-mail: shih@ini.phys.ethz.ch.

This article contains supporting information online at www.pnas.org/cgi/content/full/0909394107/DCSupplemental.

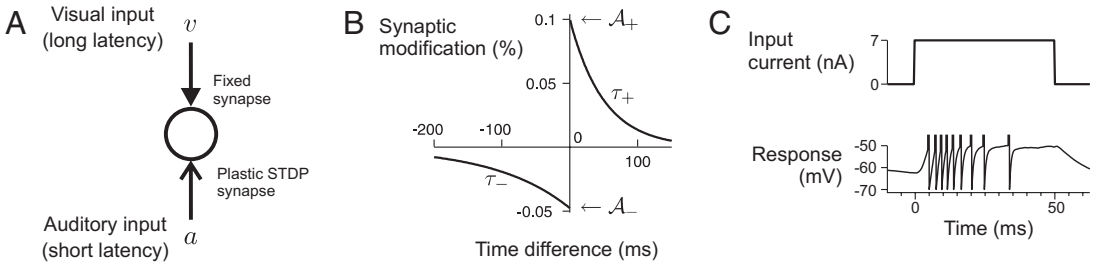

Fig. 1. A single-neuron model for instructive coding. (*A*) Neuron receives auditory input (*a*) of short latency and visual input (*v*) of longer latency. (*B*) Auditory-input synapse is subject to STDP, i.e., it strengthens when the neuron fires action potentials after presynaptic spikes (positive time difference) and weakens in the contrary case. The STDP pairing function shown has exponential tails. (*C*) Conductance-based integrate-and-fire neuron exhibits SFA, illustrated by its response to a 50 ms step input. The spike rate in response to the onset of the step input is high but then quickly adapts.

exhibits a transient response that adapts within a few milliseconds. When both inputs are simultaneously presented, however, the adaptation elicited by early auditory responses persists and leads to suppression of subsequent visual responses (Fig. 2*A*).

Mathematically, this interaction of bimodal responses can be expressed in terms of scalars A and V representing auditory and visual responses. The auditory response, A, is the average firing rate of the neuron in the time interval $[0, T]$, and the visual response, V, is the average firing rate in $[T_{\text{lat}}, T + T_{\text{lat}}]$. For short stimuli, $T \leq T_{\text{lat}}$, there is no temporal overlap between auditory and visual responses, allowing us to describe our findings unambiguously in terms of A and V.

Assuming a nonadapted state at stimulus onset, A is purely a function of auditory input. In contrast, V depends not only on the visual-input current, I_V, but also on A because of preceding adaptation. Our calculation shows that V is a linear function of both I_V and A:

$$V = c_0 + c_1 I_V - c_2 A, \qquad [1]$$

where c_0–c_2 are constants set by cellular and synaptic properties (see *Analytical Derivation*).

The linear relationship in Eq. **1** is exact under the condition that I_V is large enough to override the adaptation current and to drive spike responses in the cell. Expressed in terms of V and A, the range of validity of Eq. **1** becomes

$$V \geq c_3 A, \qquad [2]$$

where c_3 is a constant that depends on cellular/synaptic parameters (see *Analytical Derivation*). Note that when the condition in Eq. **2** is violated, the response V might be either delayed by more than T_{lat} or completely suppressed, implying a nonlinear relationship between V, A, and I_V. Nevertheless, even in this nonlinear regime, we found the linear relationship in Eq. **1** to be a good approximation of the response behavior of the cell (Fig. 2*B*).

Next, we show that under the influence of STDP, this antagonism of auditory and visual responses leads to potentiation or depression of auditory input synapses in such a way that A converges to a term proportional to I_V (assuming c_0 is small), which is the condition of alignment of auditory responses with visual inputs.

Interplay Between SFA and STDP Leads to the Delta Learning Rule. We endowed auditory synapses with a standard form of Hebbian STDP. According to the STDP rule, the joint occurrence of a presynaptic spike at time t_j and a postsynaptic spike at time t_i leads to a change in synaptic conductance, Δg, that depends solely on the time interval $\Delta t = t_i - t_j$:

$$\Delta g = g_{\max} W(\Delta t), \qquad [3]$$

where the function $W(\Delta t)$ is the STDP pairing function (Fig. 1*B*) and $g_{\max}$ is the upper limit of synaptic conductance. We chose a negative net area under the STDP pairing function, thereby imposing a tendency of the auditory synaptic strength to depress (23).

To explore the interplay between SFA and STDP, we assumed zero initial synaptic conductance ($g^A = 0$) and repeatedly stimulated the neuron with step-like auditory and visual inputs of fixed strengths and duration T. The interstimulus intervals were long, such that the adaptation conductance decayed to zero between stimulus repetitions. Initially, the neuron responded only to visual inputs but not to auditory inputs ($A = 0$). As the auditory afferents carried spikes just before the visual response, the auditory synapses started to strengthen, because afferent auditory spikes were followed by visually elicited spikes (Fig. 3*A*). With further strengthening of the auditory synapses, auditory responses started to appear. Once the neuron displayed robust auditory responses, the visual responses started to decline because of SFA. This decline, in turn, reduced the amount of synaptic potentiation, because afferent auditory spikes were now followed by fewer postsynaptic spikes. In addition, because adaptation shortened auditory responses relative to the afferent drive, there were many auditory afferent spikes that were not followed by postsynaptic spikes, imparting an additional depressing tendency in the synapses (Fig. 3*B*). In combination, there existed a balanced regime in which the synaptic depression induced by transient auditory responses equaled the potentiation induced by delayed visual responses (Fig. 3 *C* and *D*). This balanced regime did not depend on the initial synaptic conductance and was also reached when the initial conductance was set to $g_{\max}$ instead of zero.

To calculate the synaptic weight change as a function of all parameters in the model, we replaced the spike trains under the STDP pairing function with the neuron's firing rate function, $R(t)$, which represents the time-dependent spike probability (Poisson spike trains). To make calculations tractable, we simply summed over multiple spike pairs inside a given pairing window; under this condition, the total conductance change, Δg, associated with one stimulus presentation becomes the integral

$$\Delta g = g_{\max} \int_{-\infty}^{\infty} W(t')\gamma(t')\mathrm{d}t', \qquad [4]$$

where $\gamma(t') = \int_{-\infty}^{\infty} a(t)R(t+t')\mathrm{d}t$ is the cross-correlation as a function of the time lag t' between the auditory input rate function, $a(t)$, and the firing rate, $R(t)$.

When we evaluated Δg in Eq. **4** for $a(t)$, a step function with peak value a, we derived the learning rule:

$$\Delta g = g_{\max}(c_4 V - c_5 A)a, \qquad [5]$$

where the terms c_4 and c_5 depend on model details (see *Analytical Derivation*). We further transformed Eq. **5** by replacing V with I_V, using Eq. **1**, to yield

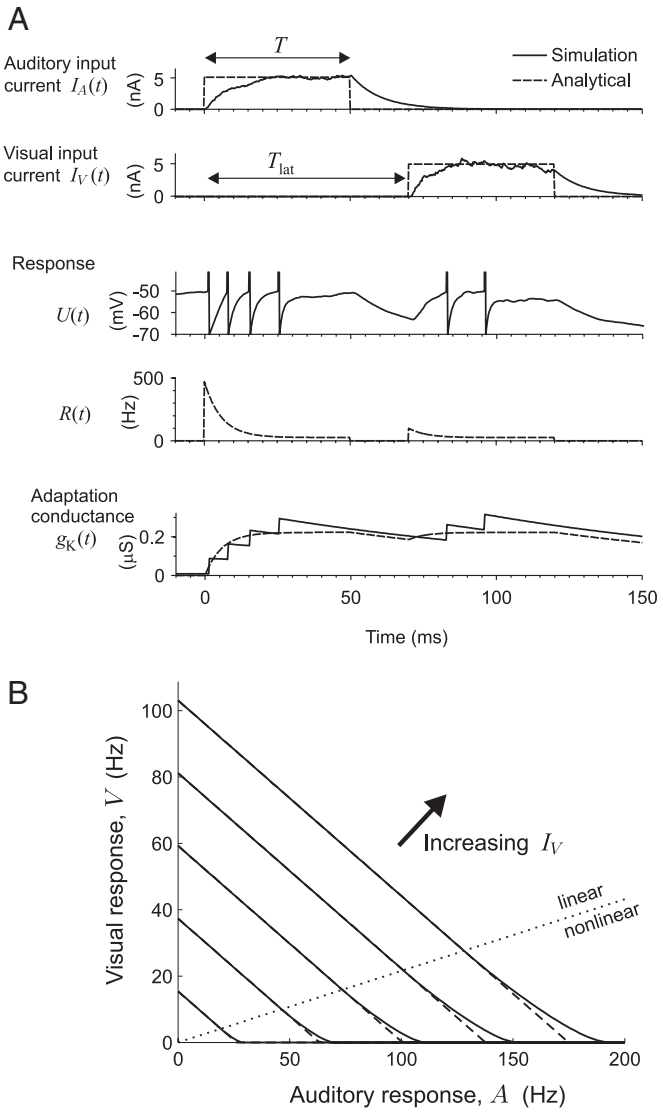

Fig. 2. Under SFA, visual responses, *V*, to a multimodal stimulus report the alignment of preceding auditory responses, *A*. (*A*) (*Top*) Auditory and visual input currents, I_A and I_V (solid lines), are approximated as step functions of duration, *T* (dashed lines). T_{lat}, visual latency. (*Middle*) Firing rate, *R*(*t*), adapts during the auditory input and leads to reduced firing during the equally strong visual input. *U*(*t*), membrane potential. (*Bottom*) Fast buildup and slow decay of the adaptation conductance, g_K. (*B*) Visual response, *V*, is a linear decreasing function of the auditory response, *A*. The different curves correspond to visual input current (I_V), varying from 0.95 to 6.35 nA in 1.35 nA increments along the direction of the arrow. This analytical relationship between *A* and *V* (Eq. **1**) is linear for large I_V values. The linear relationship is also a good approximation outside this bound (the bound of the linear range in Eq. **2** is indicated by the dotted line, and the extrapolation of the linear relationships is indicated by the dashed lines).

$$\Delta g = g_{\max}(c_6 I_V - c_7 A)a, \qquad [6]$$

which is formally equivalent to the delta rule of the perceptron learning theory. Namely, the term $(c_6 I_V - c_7 A)$ is the deviation of the auditory response, A, from the target rate $(c_6/c_7)I_V$ and corresponds to the postsynaptic error, and the term a is the presynaptic firing rate. Hence, mathematically, STDP and SFA jointly prescribe synaptic weight changes that are proportional to the postsynaptic error times the presynaptic rate. Because the delta rule corresponds to gradient descent on the square error between the neural response and the target response (12, 13), the effect of repeated application of the rule is to make auditory responses equal to visual inputs (with a fixed proportionality factor between them).

Note that Eqs. **5** and **6** are valid for a sufficiently large visual response, V [as specified in Inequality (Eq. **2**)]. Nevertheless, numerical evaluation of Eq. **4** revealed that these equations remained approximately valid even in the full-range $V \geq 0$ (Fig. 3*D*). Also, Eq. **5** was in good agreement with weight changes obtained in spiking-neuron simulations (Fig. 3 *C* and *E*).

ICX Map Formation. When we extended our model to an ICX neuron that received auditory input from pools of spatially tuned and topographically laid out neurons [mimicking the central nucleus of the inferior colliculus (ICC)], we found that, in equilibrium, ICX auditory tuning curves were approximately Gaussian-shaped and in register with visual tuning curves (Fig. 4). Hence, under STDP and SFA, the visual tuning from OT can be precisely transferred onto auditory response tuning in ICX, in excellent agreement with the delta rule (for details, see *Formation and Registration of Auditory–Visual Maps in the Avian Midbrain* in *SI Text*).

Discussion

Our work shows that SFA can be viewed as a mechanism for instructive error signaling in sensory neurons when these are driven by sparse multimodal inputs in a slow pathway and a fast pathway. SFA trades off between slow ("late arriving") responses of one modality and fast responses of another modality in an approximately linear fashion (Fig. 2*B*). The consequence is that the late sensory responses can be viewed as instructive or error signals that convey the need to respond to the earlier arriving inputs.

When we endowed early-input synapses with STDP, we found that synaptic changes were well described by the delta learning rule (21, 24); our implementation does not rely on an explicit neural representation of the error term. Rather, the error is implicitly computed through the interplay of SFA and STDP.

Our calculations showed that the emergence of the delta rule under SFA and STDP is remarkably robust. In conductance-based model neurons, the delta rule was well approximated, irrespective of cellular parameters, provided that the visual drive arrived no later than τ_+ (potentiation window size) after offset of auditory responses (or else there are no pre-post spike pairings that fall into the STDP window). Also, for adaptation to give rise to an implicit error signal (Fig. 2*B*), the adaptation time constant needed to be long enough to prevent recovery from adaptation before arrival of visual inputs (i.e., $\tau_K > \approx T_{lat}$).

Under special circumstances, when $\tau_- < \tau_+$, we found that the delta or perceptron rule can also be derived for neurons without SFA (see end of *Mathematical Derivation of the Perceptron Learning Rule* in *SI Text*). However, because $\tau_- < \tau_+$ has not been reported experimentally, it remains to be seen whether this scenario is biologically relevant.

In previous models of collicular map formation based on Hebbian plasticity (18, 25), temporal correlations and response latencies were not considered, leaving out the potential significance of delayed inputs for instructive coding. By contrast, we interpret latency differences as a computational strategy of the brain, agreeing with the notion that latency coding is very prominent in the visual system and can be found as early as in the retina (26).

In our simulations and derivations, we assumed sparseness of auditory and visual inputs (long dead time between consecutive inputs). In this regime, SFA helps to reduce a known instability of STDP (unrestrained potentiation) that arises from very brief inputs (see *SFA Helps to Reduce Unrestrained Potentiation for Short and Sparse Inputs* in *SI Text*).

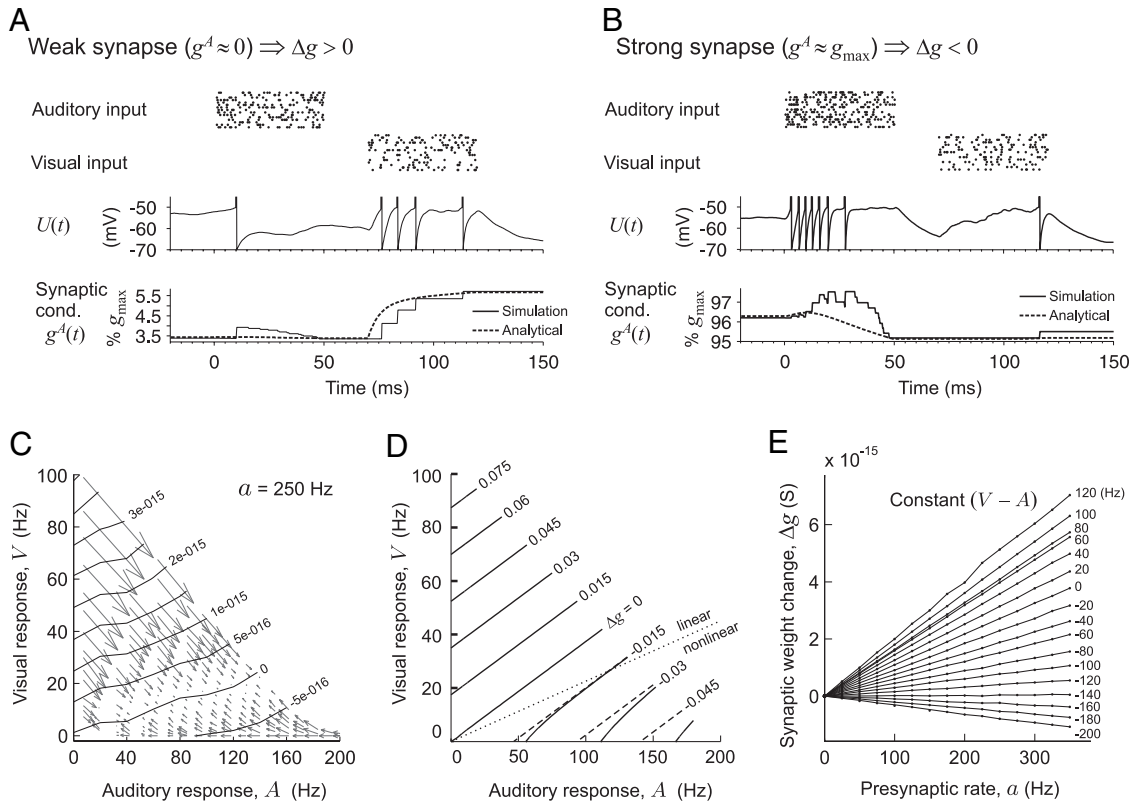

Fig. 3. The combination of STDP and SFA implements the delta learning rule. (*A*) When afferent synapses are weak, auditory inputs do not elicit auditory responses. As a result, the neuron [with membrane potential $U(t)$] responds strongly to the visual input, thus leading to strengthening of the synaptic conductance, g^A, of a representative auditory synapse. (*B*) When auditory afferent synapses are strong, the neuron's firing adaptation to auditory inputs results in more post-pre spike pairings, and thus leads to depression of synaptic strength. (*C*) Spiking-neuron simulation result of vector field illustrating the interplay between synaptic weight changes and auditory–visual responses. The lengths of the arrows are proportional to the absolute value of Δg (arbitrarily scaled units), and their directions indicate the effects Δg has on auditory responses, *A*, and visual responses, *V*. For example, an arrow pointing to the left indicates a negative weight change (depression) with the effect of reducing *A*, and an arrow pointing to the lower right indicates a positive weight change (potentiation) that increases *A* and decreases *V*. Contour lines of Δg (solid lines, in increments of 5×10^{-16} S) are roughly parallel to $bV - A$, where $b = 0.143$ is a constant. Along the contour line, 0, potentiation balances depression (equilibrium point). This plot was produced for the fixed presynaptic firing rate $a = 250$ Hz and looked qualitatively similar for values of a in the range of 50–350 Hz. (*D*) Contour lines as in *C* but based on numerical evaluation of Eq. **4**. The bound (Eq. **2**) for which the delta rule (Eq. **5**) is exact is indicated by the dotted line. For small *V*, the extrapolation of the linear relationships in Eq. **5** (dashed lines) is a good approximation of the true nonlinear behavior. (*E*) Synaptic weight changes, Δg, depend linearly on the presynaptic firing rate a (in Hz) for different values of $V - A$ (spiking-neuron simulations).

During complete absence of instructive visual inputs (e.g., at night), synaptic weights in our model decayed down to zero, in agreement with the perceptron learning rule. A mechanism to counteract such undesirable synaptic decay could arise from the existence of an additional source of delayed input to ICX neurons, with function similar to the delayed visual inputs. For example, feedback loops between the ICX and OT (27–29) could act as a delay line, giving rise to delayed auditory inputs with similar tuning as the preceding ICX auditory responses, thereby promoting synaptic stability (see also *Stability of Learned Synaptic Weights when*

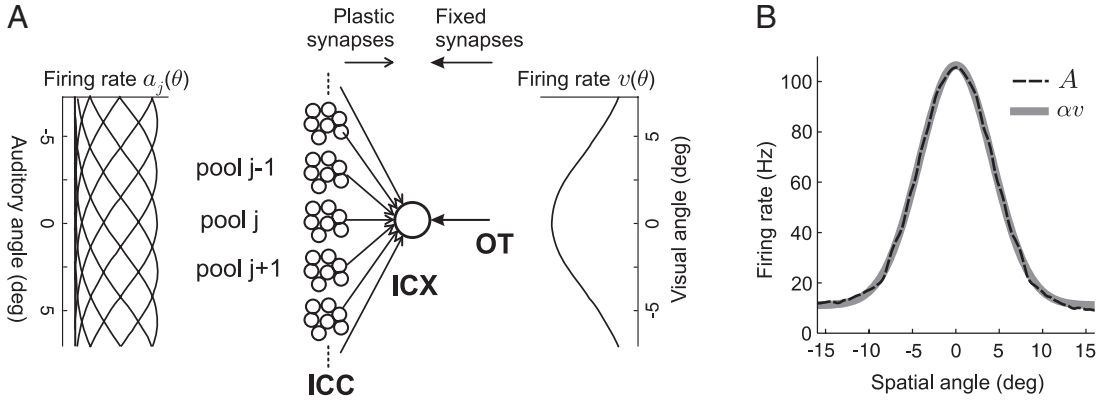

Fig. 4. Map formation in the ICX. (*A*) We model a single ICX neuron receiving auditory inputs from pools of ICC neurons and visual inputs from a pool of OT neurons. The auditory and visual tuning functions, $a(\theta)$ and $v(\theta)$, respectively, are bell-shaped. (*B*) Equilibrium ICX auditory response tuning, $A(\theta)$, (dashed line) is roughly proportional to OT tuning curves, $v(\theta)$, (full line, with a suitable scaling factor α), thereby qualifying OT inputs as perceptron-like teacher signals.

Visual Inputs Are Absent in *SI Text*). Such a scenario could also apply to cortex, where SFA and STDP coexist (30–33) and where decay of feedforward connections could be prevented by delayed inputs arising from feedback loops via higher cortical areas (34, 35).

In computational learning theories, STDP has been linked to temporal difference learning (36) and to maximization of mutual information (37). Here, we extend this list of computational functions of STDP to include gradient-descent error minimization. By establishing a connection between the delta rule and simple neuron biophysics, our work strengthens the links between computational learning rules and adaptation and plasticity in biological systems. Along with similar efforts (38), our work suggests that learning rules derived from computational insights may be more compatible with simple neuron biophysics than previously thought.

Methods

Integrate-and-Fire Neurons. The leaky integrate-and-fire model (ICX) neuron with membrane potential $U(t)$ satisfies

$$C_m\frac{dU}{dt} = -I_L + I_s - I_K + I_b, \qquad [7]$$

where C_m = 0.5 nF is the membrane capacitance, $I_L = g_L(U - E_L)$ is the leakage current, I_s is the total excitatory synaptic input current from auditory and visual afferents, I_K is a firing-rate adaptation current, and I_b is a background input current (see *Additional Details on Methods* in *SI Text*). The threshold potential is E_θ = −50 mV, the reset/resting potential is E_L = −70 mV, and the leakage conductance is g_L = 20 nS. When the membrane potential reaches E_θ, the neuron produces an action potential and the membrane potential is reset to E_L. There is no refractory period.

SFA. The adaptation current $I_K = g_K(U - E_K)$ in Eq. **7** models calcium-activated potassium channels, where g_K is the potassium conductance and E_K = −70 mV is the potassium reversal potential. The potassium conductance, g_K, is a step-and-decay function driven by the neuron's spike train, $\rho(t)$ (sum of delta functions):

$$\frac{dg_K}{dt} + \frac{1}{\tau_K}g_K = \Delta_{g_K}\rho(t), \qquad [8]$$

with increment Δ_{g_K} = 80 nS on every spike, and a decay time constant τ_K = 110 ms (Fig. 2*A*). The decay time constant was inferred from the work of Gutfreund and Knudsen (20).

Auditory and Visual Inputs. The synaptic current, I_s, onto the neuron stems from populations of visual and auditory afferents:

$$I_s = \sum_j g_j^A s_j^A(t)(U - E_{ex}) + g^V s^V(t)(U - E_{ex}), \qquad [9]$$

where $s_j^A(t)$ is the synaptic activation of the *jth* auditory afferent and $s^V(t)$ is the summed synaptic activation from a pool of visual neurons. The connection strength, g_j^A, is modified according to an STDP rule and constrained to $0 \le g_j^A \le g_{max}$, with g_{max} = 1.25 nS. The visual-input synapses are of fixed strength, g^V = 3 nS; because they convey inputs from independently firing visual neurons, we represent their synaptic activation variables by the single variable $s^V(t)$, describing the entire pool. All synapses are excitatory with reversal potential, E_{ex} = 0 mV. Synaptic activations, $s(t)$, are step-and-decay functions. Each time an input spike arrives, $s(t)$ is incremented by 1. Between spikes, $s(t)$ decays exponentially to zero according to $\tau_s ds/dt = -s$, with a time constant of τ_s = 10 ms (39).

The auditory and visual step-input amplitudes (firing rates) for simulations in Figs. 2 and 3 varied from a = 0–350 Hz and v = 0–250 Hz, respectively.

STDP. The STDP pairing function in Eq. **3** is defined by $W(\Delta t) = \mathcal{A}_+ e^{-\Delta t/\tau_+}$ for $\Delta t > 0$ and $W(\Delta t) = -\mathcal{A}_- e^{\Delta t/\tau_-}$ for $\Delta t \le 0$. We set the half-widths of the pairing function to τ_+ = 50 ms and τ_- = 110 ms and the amount of potentiation per spike to $\mathcal{A}_+$ = 0.001. The amount of depression per spike was chosen according to the relationship $B = \mathcal{A}_-\tau_-/\mathcal{A}_+\tau_+ = 1.05$, which implies that the net area under W is negative. The half-widths of the pairing function were chosen to be within the range of the correlation time of auditory and visual inputs. The value for τ_- on the order of 100 ms is typical in cortex (40, 41), whereas measured cortical values for τ_+ tend to be smaller than 50 ms (on the order of 20 ms). However, our findings also applied to such small τ_+ values, provided that τ_- was small as well or that auditory stimuli were sufficiently far away from the animal (>10 m) to provide for pre-post spike pairing within τ_+ (Fig. S8).

Note on Parameter Choice. In our ICX–neuron simulations, we tried to constrain model parameters by existing data. When this was not possible, we adhered to the constraint that simulated ICX rates should match those of experimentally recorded ICX responses (22). To produce Figs. 2*B*, 3 *C–E*, and 4, we set the visual stimulus duration to 50 ms and the auditory stimulus duration to 70 ms. Our results were insensitive to these and similar differential changes of auditory and visual stimulus durations.

Analytical Derivation. The perceptron learning rule in Eq. **5** is a generic consequence of the interplay between adaptation and STDP and does not depend on model details. In fact, Eqs. **1** and **5** can be derived analytically by simplifying the conductance-based model equations (Eqs. **7**–**9**) using the method of time averaging (24) and simplifying Poissonian assumptions (42, 43). In the following, we briefly outline this derivation assuming that $E_K = E_L$ and that the duration, T, of auditory–visual stimuli is smaller than the visual latency ($T \le T_{lat}$). This latter assumption implies that the neuron's auditory and visual responses, A and V, do not temporally overlap, and thus are unambiguously defined. The detailed derivation is provided in *SI Text* (*Mathematical Derivation of the Perceptron Learning Rule*).

Derivation of $V = c_0 + c_1 I_V - c_2 A$. The method of time averaging consists of replacing the neuron's spike train, $\rho(t)$, in Eq. **8** by the average firing rate, $R(\cdot)$, which is a good approximation, provided that the time scale of spike-frequency adaptation (τ_K = 110 ms) is much longer than the membrane time constant (τ_m = 25 ms). For integrate-and-fire neurons (Eq. **7**), this firing-rate function, $R(I)$, is an approximate threshold-linear function of the total membrane current $I = g_L(E_L - E_\theta) + g_K(E_L - E_\theta) + I_V + I_A$:

$$R(I) = \begin{cases} \dfrac{I}{C_m(E_\theta - E_L)} & \text{for } I \ge 0, \\ 0 \quad \text{otherwise,} \end{cases} \qquad [10]$$

where I_A and I_V are the synaptic input currents from auditory and visual afferents, respectively, in Eq. **9**. More specifically, Eq. **10** is an excellent linear approximation of the exact (nonlinear) expression for $R(I)$ for large suprathreshold input currents: $I \gg I_\theta$ where $I_\theta = (g_L + g_K)(E_\theta - E_L)$ is the sum of leak and adaptation currents at firing threshold (absolute values)

Under the approximation (Eq. **10**), the adaptation conductance, $g_K(t)$, in Eq. **8** turns into a low-pass-filtered copy of the average firing rate, $R(t)$; mathematically, $g_K(t)$ obeys a simple first-order linear differential equation. When we analytically solve this linear differential equation for $g_K(t)$ and $R(t)$ and then compute $A = \int_0^T R(t)dt$ and $V = \int_{T_{lat}}^{T+T_{lat}} R(t)dt$, we find the desired linear relationship between A, V, and I_V, as given by Eq. **1**, with

$$c_0 = -\frac{cg_L}{C_m}, c_1 = \frac{c}{C_m(E_\theta - E_L)}, \text{ and } c_2 = \frac{\tau_{eff}^2}{c\tau_1 T}e^{-\frac{T_{lat}-T}{\tau_K}},$$

where $1/\tau_{eff} = 1/\tau_1 + 1/\tau_K$, $\tau_1 = C_m/\Delta_{g_K}$, and $c = \tau_{eff}/\tau_K + \tau_{eff}^2/\tau_1 T$. Note that V in Eq. **1** depends linearly on the constant visual input v, because to first-order approximation I_V is proportional to v (i.e., $I_V = -\langle U\rangle g^V \tau_s N v$, where $\langle U\rangle$ is the average ICX membrane voltage and N is the number of neurons in the OT pool). For our choice of parameters, the offset c_0 in Eq. **1** can be neglected because it is small (6 Hz) when compared with the range of v (1–250 Hz). The linear relationship in Eq. **1** is exact only in a range of sufficiently large visual responses [Inequality (Eq. **2**)] because of the threshold nonlinearity in Eq. **10**. In practice, however, we found that Eq. **1** provides a reasonably good approximation of visual responses as a function of preceding auditory responses also in the full range, $V \ge 0$ (Fig. 2*B*).

Derivation of $V \ge c_3 A$ as the Range of Linear Behavior. For $I_V \ge I_\theta$, the neuron immediately responds to the visual input in spite of its adapted state; in such a case, the integral $V = \int_{T_{lat}}^{T+T_{lat}} R(t)dt$ is straightforward to compute and leads to a linear relationship between A and V. Solving the differential equation for g_K, we find that its value, $g_K = Ae^{-\frac{T_{lat}-T}{\tau_K}} C_m\tau_{eff}/c\tau_1$, just before the arrival of the visual input is a function of the auditory response, A.

Combining this with the fact that V is linear in I_V, using Eq. **1**, we arrive at Inequality (Eq. **2**), with the constant c_3 given by

$$c_3 = \left(\frac{\tau_{\text{eff}}}{\tau_1} - \frac{\tau_{\text{eff}}^2}{c\tau_1 T}\right) e^{-\frac{T_{\text{lat}}-T}{\tau_K}}.$$

Note that when $I_V < I_\theta$, the response V is either delayed by more than T_{lat} or completely suppressed and the relationship between A and V becomes nonlinear.

Derivation of $\Delta g = g_{\max}(c_4 V - c_5 A)a$. Assuming step functions for inputs $a(t)$ and $v(t)$, the neuron's response, $R(t)$, is a simple sum of constants and exponentials in time, t. As a consequence, the integration in Eq. **4** can be easily performed, and we find the desired perceptron learning rule of Eq. **5**, with constants c_4 and c_5 given by

$$c_4 = \mathcal{A}_+ \frac{\tau_{\text{eff}}\tau_+^2 e^{-\frac{T_{\text{lat}}}{\tau_+}}}{c}\left[\frac{4\sinh^2\left(\frac{T}{2\tau_+}\right)}{\tau_K} + \frac{\tau_{\text{eff}}(e^{T/\tau_+}-1)}{\tau_1(\tau_+ + \tau_{\text{eff}})}\right],$$

$$c_5 = -c_2 c_4 - \mathcal{A}_+ \frac{\tau_{\text{eff}}\tau_+}{c}\left[\frac{T(1-B) + \tau_+(e^{-T/\tau_+}-1) - B\tau_-(e^{-T/\tau_-}-1)}{\tau_K} + \frac{\tau_{\text{eff}}}{\tau_1}\left(\frac{\tau_{\text{eff}} - \tau_+ e^{-\frac{T_{\text{lat}}-T}{\tau_K}} e^{-\frac{T_{\text{lat}}}{\tau_+}}(e^{T/\tau_+}-1)}{\tau_+ + \tau_{\text{eff}}} - B\left(1 - \frac{\tau_- e^{-T/\tau_-}}{\tau_- - \tau_{\text{eff}}}\right)\right)\right]$$

ACKNOWLEDGMENTS. P.D. is partially funded by the Zentrum fuer Neurowissenschaften Zurich.

1. Karklin Y, Lewicki MS (2005) A hierarchical Bayesian model for learning nonlinear statistical regularities in nonstationary natural signals. *Neural Comput* 17:397–423.
2. Olshausen BA, Field DJ (1996) Emergence of simple-cell receptive field properties by learning a sparse code for natural images. *Nature* 381:607–609.
3. Hahnloser RH (2003) Emergence of neural integration in the head-direction system by visual supervision. *Neuroscience* 120:877–891.
4. Robinson DA (1989) Integrating with neurons. *Annu Rev Neurosci* 12:33–45.
5. Xie X, Hahnloser RH, Seung HS (2002) Selectively grouping neurons in recurrent networks of lateral inhibition. *Neural Comput* 14:2627–2646.
6. Atwal GS (2004) Dynamic plasticity in coupled avian midbrain maps. *Phys Rev E* 70: 061904.
7. Rothman JS, Cathala L, Steuber V, Silver RA (2009) Synaptic depression enables neuronal gain control. *Nature* 457:1015–1018.
8. Benda J, Herz AV (2003) A universal model for spike-frequency adaptation. *Neural Comput* 15:2523–2564.
9. Benda J, Longtin A, Maler L (2005) Spike-frequency adaptation separates transient communication signals from background oscillations. *J Neurosci* 25:2312–2321.
10. Brainard MS, Knudsen EI (1993) Experience-dependent plasticity in the inferior colliculus: A site for visual calibration of the neural representation of auditory space in the barn owl. *J Neurosci* 13:4589–4608.
11. Knudsen EI, Brainard MS (1991) Visual instruction of the neural map of auditory space in the developing optic tectum. *Science* 253:85–87.
12. Rosenblatt F (1958) The perceptron: A probabilistic model for information storage and organization in the brain. *Psychol Rev* 65:386–408.
13. Widrow B, Hoff ME (1960) Adaptive switching circuits. *Institute of Radio Engineers WESCON Convention Record* (Institute of Radio Engineers, New York), pp 96–104.
14. Brunel N, Hakim V, Isope P, Nadal JP, Barbour B (2004) Optimal information storage and the distribution of synaptic weights: Perceptron versus Purkinje cell. *Neuron* 43: 745–757.
15. Fiete IR, Fee MS, Seung HS (2007) Model of birdsong learning based on gradient estimation by dynamic perturbation of neural conductances. *J Neurophysiol* 98: 2038–2057.
16. Seriès P, Latham PE, Pouget A (2004) Tuning curve sharpening for orientation selectivity: Coding efficiency and the impact of correlations. *Nat Neurosci* 7:1129–1135.
17. Davison AP, Frégnac Y (2006) Learning cross-modal spatial transformations through spike timing-dependent plasticity. *J Neurosci* 26:5604–5615.
18. Friedel P, van Hemmen JL (2008) Inhibition, not excitation, is the key to multimodal sensory integration. *Biol Cybern* 98:597–618.
19. Legenstein R, Naeger C, Maass W (2005) What can a neuron learn with spike-timing-dependent plasticity? *Neural Comput* 17:2337–2382.
20. Gutfreund Y, Knudsen EI (2006) Adaptation in the auditory space map of the barn owl. *J Neurophysiol* 96:813–825.
21. Ermentrout B (1998) Linearization of F-I curves by adaptation. *Neural Comput* 10: 1721–1729.
22. Gutfreund Y, Zheng W, Knudsen EI (2002) Gated visual input to the central auditory system. *Science* 297:1556–1559.
23. Song S, Miller KD, Abbott LF (2000) Competitive Hebbian learning through spike-timing-dependent synaptic plasticity. *Nat Neurosci* 3:919–926.
24. Ermentrout B (1994) Reduction of conductance-based models with slow synapses to neural nets. *Neural Comput* 6:679–695.
25. Witten IB, Knudsen EI, Sompolinsky H (2008) A Hebbian learning rule mediates asymmetric plasticity in aligning sensory representations. *J Neurophysiol* 100: 1067–1079.
26. Gollisch T, Meister M (2008) Rapid neural coding in the retina with relative spike latencies. *Science* 319:1108–1111.
27. Reches A, Gutfreund Y (2008) Stimulus-specific adaptations in the gaze control system of the barn owl. *J Neurosci* 28:1523–1533.
28. Winkowski DE, Knudsen EI (2007) Top-down control of multimodal sensitivity in the barn owl optic tectum. *J Neurosci* 27:13279–13291.
29. Rodriguez-Contreras A, Liu XB, DeBello WM (2005) Axodendritic contacts onto calcium/calmodulin-dependent protein kinase type II-expressing neurons in the barn owl auditory space map. *J Neurosci* 25:5611–5622.
30. Ahmed B, Anderson JC, Douglas RJ, Martin KA, Whitteridge D (1998) Estimates of the net excitatory currents evoked by visual stimulation of identified neurons in cat visual cortex. *Cereb Cortex* 8:462–476.
31. Fuhrmann G, Markram H, Tsodyks M (2002) Spike frequency adaptation and neocortical rhythms. *J Neurophysiol* 88:761–770.
32. Meliza CD, Dan Y (2006) Receptive-field modification in rat visual cortex induced by paired visual stimulation and single-cell spiking. *Neuron* 49:183–189.
33. Schuett S, Bonhoeffer T, Hübener M (2001) Pairing-induced changes of orientation maps in cat visual cortex. *Neuron* 32:325–337.
34. Johnson RR, Burkhalter A (1996) Microcircuitry of forward and feedback connections within rat visual cortex. *J Comp Neurol* 368:383–398.
35. Douglas RJ, Martin KA (2004) Neuronal circuits of the neocortex. *Annu Rev Neurosci* 27:419–451.
36. Rao RP, Sejnowski TJ (2001) Spike-timing-dependent Hebbian plasticity as temporal difference learning. *Neural Comput* 13:2221–2237.
37. Toyoizumi T, Pfister JP, Aihara K, Gerstner W (2005) Generalized Bienenstock-Cooper-Munro rule for spiking neurons that maximizes information transmission. *Proc Natl Acad Sci USA* 102:5239–5244.
38. Sprekeler H, Michaelis C, Wiskott L (2007) Slowness: An objective for spike-timing-dependent plasticity? *PLOS Comput Biol* 3:1136–1148.
39. Feldman DE, Knudsen EI (1994) NMDA and non-NMDA glutamate receptors in auditory transmission in the barn owl inferior colliculus. *J Neurosci* 14:5939–5958.
40. Froemke RC, Poo MM, Dan Y (2005) Spike-timing-dependent synaptic plasticity depends on dendritic location. *Nature* 434:221–225.
41. Feldman DE (2000) Timing-based LTP and LTD at vertical inputs to layer II/III pyramidal cells in rat barrel cortex. *Neuron* 27:45–56.
42. Drew PJ, Abbott LF (2006) Extending the effects of spike-timing-dependent plasticity to behavioral timescales. *Proc Natl Acad Sci USA* 103:8876–8881.
43. Kempter R, Gerstner W, van Hemmen JL (1999) Hebbian learning and spiking neurons. *Phys Rev E* 59:4498–4514.